Bone Enhancement in Ultrasound Based on 3D Local Spectrum Variation for Percutaneous Scaphoid Fracture Fixation

Emran Mohammad Abu Anas[1(✉)], Alexander Seitel[1], Abtin Rasoulian[1],
Paul St. John[2], Tamas Ungi[3], Andras Lasso[3], Kathryn Darras[4], David Wilson[5],
Victoria A. Lessoway[6], Gabor Fichtinger[3], Michelle Zec[2], David Pichora[2],
Parvin Mousavi[3], Robert Rohling[1,7], and Purang Abolmaesumi[1]

[1] Electrical and Computer Engineering, University of British Columbia,
Vancouver, BC, Canada
emrana@ece.ubc.ca
[2] Kingston General Hospital, Kingston, ON, Canada
[3] School of Computing, Queen's University, Kingston, ON, Canada
[4] Vancouver General Hospital, Vancouver, BC, Canada
[5] Orthopaedics and Centre for Hip Health and Mobility,
University of British Columbia, Vancouver, BC, Canada
[6] BC Women's Hospital, Vancouver, BC, Canada
[7] Mechanical Engineering, University of British Columbia, Vancouver, BC, Canada

Abstract. This paper proposes a 3D local phase-symmetry-based bone enhancement technique to automatically identify weak bone responses in 3D ultrasound images of the wrist. The objective is to enable percutaneous fixation of scaphoid bone fractures, which occur in 90 % of all carpal bone fractures. For this purpose, we utilize 3D frequency spectrum variations to design a set of 3D band-pass Log-Gabor filters for phase symmetry estimation. Shadow information is also incorporated to further enhance the bone surfaces compared to the soft-tissue response. The proposed technique is then used to register a statistical wrist model to intraoperative ultrasound in order to derive a patient specific 3D model of the wrist bones. We perform a cadaver study of 13 subjects to evaluate our method. Our results demonstrate average mean surface and Hausdorff distance errors of 0.7 mm and 1.8 mm, respectively, showing better performance compared to two state-of-the art approaches. This study demonstrate the potential of the proposed technique to be included in an ultrasound-based percutaenous scaphoid fracture fixation procedure.

Keywords: Bone enhancement · Scaphoid fracture · Phase symmetry · Log-Gabor filters · Shadow map

1 Introduction

Scaphoid fracture is the most probable outcome of wrist injury and it often occurs due to sudden fall on an outstretched arm. To heal the fracture, casting

is usually recommended which immobilizes the wrist in a short arm cast. The typical healing time is 10–12 weeks, however, it can be longer especially for a fracture located at the proximal pole of the scaphoid bone [8]. Better outcome and faster recovery are normally achieved through open (for displaced fracture) or percutaneous (for non-displaced fracture) surgical procedure, where a surgical screw is inserted along the longest axis of the fractured scaphoid bone within a clinical accuracy of 2 mm [7].

In the percutaneous surgical approach for scaphoid fractures, fluoroscopy is usually used to guide the screw along its desired drill path. The major drawbacks of a fluoroscopic guidance are that only a 2D projection view of a 3D anatomy can be used and that the patient and the personnel working in the operating room are exposed to radiation. For reduction of the X-ray radiation exposure, a camera-based augmentation technique [10] can be used. As an alternative to fluoroscopy, 3D ultrasound (US)-based procedure [2,3] has been suggested, mainly to allow real-time 3D data for the navigation. However, the main challenge of using US in orthopaedics lies in the enhancement of weak, dis-connected, blurry and noisy US bone responses.

The detection/enhancement of the US bone responses can be broadly categorized into two groups: intensity-based [4] and phase-based approaches [2,5,6]. A review of the literature of these two approaches suggests the phase-based approaches have an advantage where there are low-contrast or variable bone responses, as often observed in 3D US data. Hacihaliloglu *et al.* [5,6] proposed a number of phase-based bone enhancement approaches using a set of quadrature band-pass (Log-Gabor) filters at different scales and orientations. These filters assumed isotropic frequency responses across all orientations. However, the bone responses in US have a highly directional nature that in turn produce anisotropic frequency responses in the frequency domain. Most recently, Anas *et al.* [2] presented an empirical wavelet-based approach to design a set of 2D anisotropic band-pass filters. For bone enhancement of a 3D US volume, that 2D approach could be applied to individual 2D frames of a given US volume. However, as a 2D-based approach, it cannot take advantage of correlations between adjacent US frames. As a result, the enhancement is affected by the spatial compounding errors and the errors resulting from the beam thickness effects [5].

In this work, we propose to utilize local 3D Fourier spectrum variations to design a set of Log-Gabor filters for 3D local phase symmetry estimation applied to enhance the wrist bone response in 3D US. In addition, information from the shadow map [4] is utilized to further enhance the bone response. Finally, a statistical wrist model is registered to the enhanced response to derive a patient-specific 3D model of the wrist bones. A study consisting of 13 cadaver wrists is performed to determine the accuracy of the registration, and the results are compared with two previously published bone enhancement techniques [2,5].

2   Methods

Bone responses in US are highly directional with respect to the direction of scanning, i.e., the width of the bone response along the scanning direction is

significantly narrower than along other directions. As a result, the magnitude spectrum of an US volume has wider bandwidth along the scanning direction than along other directions. Most of the existing phase-based approaches [5,6] employ isotropic filters (having same bandwidths and center frequencies) across different directions for the phase symmetry estimation. However, the isotropic filter bank may not be appropriate to extract the phase symmetry accurately from an anisotropic magnitude spectrum. In contrast to those approaches, here, we account for the spectrum variations in different directions to design an anisotropic 3D Log-Gabor filter bank for an improved phase symmetry estimation.

2.1 Phase Symmetry Estimation

The 3D local phase symmetry estimation starts with dividing a 3D frequency spectrum into different orientations (example in Fig. 1(a)). A set of orientational filters are used for this purpose, where the frequency response of each filter is defined as a multiplication of azimuthal ($\Phi(\phi)$) and polar ($\Theta(\theta)$) filters:

$$O(\phi, \theta) = \Phi(\phi) \times \Theta(\theta) = \exp\left(-\frac{(\phi - \phi_0)^2}{2\sigma_\phi}\right) \times \exp\left(-\frac{(\theta - \theta_0)^2}{2\sigma_\theta}\right), \qquad (1)$$

where the azimuthal angle ϕ $(0 \leq \phi \leq 2\pi)$ measures the angle in the xy-plane from the positive x-axis in counter-clockwise direction, and the polar angle θ $(0 \leq \theta \leq \pi)$ indicates the angle from the positive z-axis. ϕ_0 and θ_0 indicate the center of the orientation, and σ_ϕ and σ_θ represent the span/bandwidth of the orientation (Fig. 1(a)). The purpose of the polar orientational filter is to divide the 3D spectrum into different cones, and the azimuthal orientational filter further divides each cone into different sub-spectrums/orientations (Fig. 1(a)).
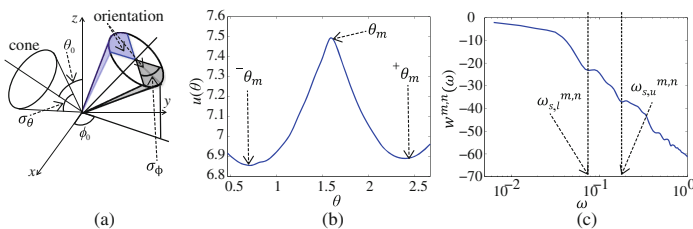

Fig. 1. Utilization of the spectrum variation in local phase symmetry estimation. (a) A 3D frequency spectrum is divided into different cones, and each segmented cone is further partitioned into different orientations. (b) The variation of spectrum strength over the polar angle. (c) The variation of spectrum strength over the angular frequency.

After selection of a particular orientation, band-pass Log-Gabor filters are applied at different scales. Mathematically, the frequency response of a Log-Gabor filter is defined as below:

$$R(\omega) = \exp\left(-\frac{(\ln(\frac{\omega}{\omega_0}))^2}{2(\ln(\kappa))^2}\right), \qquad (2)$$

where $\omega\,(0 \leq \omega \leq \sqrt{3}\pi)$ represents the angular frequency, ω_0 represents the peak tuning frequency, and $0 < \kappa < 1$ is related to the octave bandwidth. Finally, the frequency response of a band-pass Log-Gabor filter at a particular orientation can be expressed as: $F(\omega, \phi, \theta) = R(\omega)O(\phi, \theta)$.

2.2   Enhancement of Bone Responses in US

The bone enhancement starts with the estimation of the parameters for the orientational filter $(\phi_0, \theta_0, \sigma_\phi, \sigma_\theta)$ for each orientation (Sect. 2.2.1). The estimation of the Log-Gabor filter parameters for each orientation is presented in Sect. 2.2.2. The subsequent bone surface extraction is described afterward (Sect. 2.2.3).

2.2.1   Parameters for Orientational Filter

The first step is to compute spherical Fourier transform (FT) $P(\omega, \phi, \theta)$ from a given US volume. To do so, the 3D conventional FT in rectangular coordinates is calculated, followed by transforming them into spherical coordinates. For segmentation of the spectrum into different cones, we compute the strength of the spectrum along the polar angle coordinate as: $u(\theta) = \sum_{\omega=0}^{\sqrt{3}\pi} \sum_{\phi=0}^{2\pi} \log(|P(\omega, \phi, \theta)|)$. An example $u(\theta)$ is demonstrated in Fig. 1(b). The locations θ_m of the maxima of $u(\theta)$ are detected, where $m = 1, 2, ..., M$, and M is the total number of detected maxima. For each θ_m, the detected left and right minima are represented as $^-\theta_m$ and $^+\theta_m$ (shown in Fig. 1(b)), and the difference between these two minima positions is estimated as: $\sigma_{\theta,m} =^+ \theta_m -^- \theta_m$. Note that each detected maxima corresponds to a cone in the 3D frequency spectrum, i.e., the total number of cones is M, the center and the bandwidth of the m-th cone are θ_m and $\sigma_{\theta,m}$, respectively.

Subsequently, each segmented cone is further divided into different subspectrums. To do so, the strength of the spectrum is calculated along the azimuthal angle within a particular cone (say, m-th cone), followed by the maxima and corresponding two neighboring minima as before. Then, the center ϕ_n^m and the bandwidth $\sigma_{\phi,n}^m$ of the n-th sub-spectrum within m-th cone are calculated.

2.2.2   Parameters for Log-Gabor Filters

For estimation of the Log-Gabor filter parameters at each orientation, the spectrum strength is calculated within that orientation as: $w^{m,n}(\omega) = \sum_\theta \sum_\phi 20 \log(|P(\omega, \phi, \theta)|)$ dB. A segmentation of $w^{m,n}(\omega)$ is performed [2] to estimate the parameters of the Log-Gabor filters at different scales. The lower $\omega_{s,l}^{m,n}$ and upper $\omega_{s,u}^{m,n}$ cut-off frequencies for a scale s are determined from $w^{m,n}(\omega)$ (an example is shown in Fig. 1(c)), where, $1 \leq s \leq S^{m,n}, S^{m,n}$ is the total number of scales at n-th orientation within m-th cone. The right subscripts 'l' and 'u' indicate the lower and upper cut-off frequencies. The parameters of the Log-Gabor filters (ω_0 and κ) can be directly calculated

from the lower and upper cut-off frequencies as: $\omega_{s,0}^{m,n} = \sqrt{\omega_{s,l}^{m,n} \omega_{s,u}^{m,n}}$ and $\kappa_s^{m,n} = \exp(-0.25 \log_2\left(\frac{\omega_{u,l}^{m,n}}{\omega_{s,l}^{m,n}}\right) \sqrt{2\ln 2})$.

2.2.3 Bone Surface Extraction

The above estimated filter parameters are then utilized to compute the frequency responses of the orientational and Log-Gabor filters using Eqs. (1)-(2). These filters are subsequently used in 3D phase symmetry estimation [5]. As local phase symmetry also enhances other anatomical interfaces having symmetrical responses, shadow information is utilized to suppress those responses from other anatomies. A shadow map is estimated for each voxel by weighted summation of the intensity values of all voxels beneath [4]. The product of the shadow map with the phase symmetry is defined as the bone response (BR) in this work, which has a range from 0 to 1. To construct a target bone surface, we use a simple thresholding with a threshold of T_{bone} on the BR volume to detect the bones in the US volume. An optimized selection of the threshold is not possible due to a smaller sample size (13) in this work, therefore, an empirical threshold value of 0.15 is chosen.

2.3 Registration of a Statistical Wrist Model

A multi-object statistical wrist shape+scale+pose model is developed based on the idea in [1] to capture the main modes of shape, scale and pose variations of the wrist bones across a group of subjects at different wrist positions. For the training during the model development, we use a publicly available wrist database [9]. For registration of the model to a target point cloud, a multi-object probabilistic registration is used [11]. The sequential registration is carried out in two steps: (1) the statistical model is registered to a preoperative CT acquired at neutral wrist position, and (2) a subsequent registration of the model to the extracted bone surface in US acquired at a non-neutral wrist position. Note that in the second step only pose coefficients are optimized to capture the pose differences between CT and US. Note that the pose model in [1] captures both the rigid-body and scale variations; however, in this work we use two different models (pose and scale, respectively) to capture those variations. The key idea behind separation of the scale from the rigid-body motion is to avoid the scale optimization during the US registration, as the scale estimation from a limited view of the bony anatomy in US may introduce additional registration error.

3 Experiments, Evaluation and Results

A cadaver experiment including 13 cadaver wrists was performed for evaluation as well as comparison of our proposed approach with two state-of-the art techniques: a 2D empirical wavelet based local phase symmetry (EWLPS) [2] and a 3D local phase symmetry (3DLPS) [5] methods.

3.1   Experimental Setup

For acquisition of US data from each cadaver wrist, a motorized linear probe (Ultrasonix 4D L14-5/38, Ultrasonix, Richmond, BC, Canada) was used with a frequency of 10 MHz, a depth of 40 mm and a field-of-view of 30° focusing mainly on the scaphoid bone. A custom-built wrist holder was used to keep the wrist fixed at extension position (suggested by expert hand surgeons) during scanning. To obtain a preoperative image and a ground truth of wrist US bone responses, CTs were acquired at neutral and extension positions, respectively, for all 13 cadaver wrists. An optical tracking system equipped with six fiducial markers was used to track the US probe.

3.2   Evaluation

To generate the ground truth wrist bone surfaces, CTs were segmented manually using the Medical Imaging Interaction Toolkit. Fiducial-based registration was used to align the segmented CT with the wrist bone responses in US. We also needed a manual adjustment afterward to compensate the movement of the wrist bones during US acquisition due to the US probe's pressure on the wrist. The manual translational adjustment was mainly performed along the direction of the US scanning axis by registering the CT bone surfaces to the US bone responses.

   For evaluation, we measured the mean surface distance error (mSDE) and maximum surface (Hausdorff) distance error (mxSDE) between the registered and reference wrist bone surfaces. The surface distance error (SDE) at each point in the registered bone surface is defined as its Euclidean distance to the closest neighboring point in the reference surface. mSDE and mxSDE are defined as the average and maximum of SDEs across all vertices, respectively. We also recorded the run-times of the three bone enhancement techniques from unoptimized MATLAB^{TM} (Mathworks, Natick, MA, USA) code on an Intel Core i7-2600M CPU at 3.40 GHz for an US volume of size of $57.3 \times 36.45 \times 32.7 \, mm^3$ with a pixel spacing of 0.4 mm in all dimensions.

3.3   Results

Table 1 reports a comparative result of our approach with respect to the EWLPS and 3DLPS methods. For each bone enhancement technique, a consistent threshold value that provides the least error is used across 13 cadaver cases.

Table 1. Comparative results of the proposed approach.

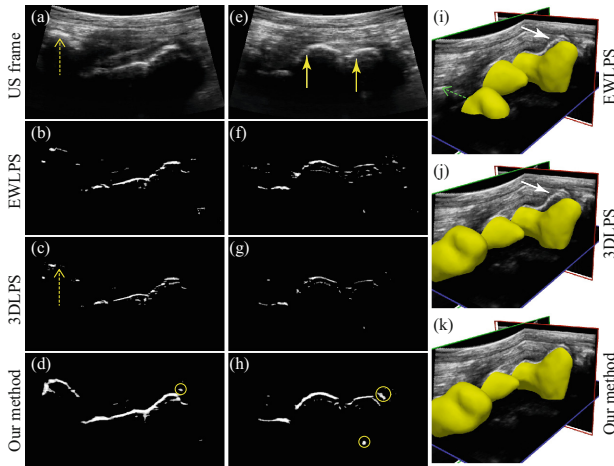| Method	mSDE (mm)	mxSDE (mm)	Run-time (sec)
Our	0.7 ± 0.2	1.8 ± 0.3	11
EWLPS	0.8 ± 0.2	2.5 ± 0.5	4
3DLPS	0.9 ± 0.3	2.3 ± 0.4	10

Fig. 2. Results of the proposed, EWLPS and 3DLPS methods. (a-h) Example sagittal US frames are shown in (a), (e). The corresponding bone enhancement are demonstrated in (b-d), (f-h). The differences in the enhancement are prominent in the surfaces marked by arrows. (i-k) Example registration results of the statistical model to US for three different methods.

Figure 2 demonstrates the significant improvement we obtain in bone enhancement quality using our proposed method over the two competing techniques. Two example US sagittal slices are demonstrated in Figs. 2(a), (e), and the corresponding bone enhancement are shown below. The registered atlases superimposed on the US volume are displayed in Figs. 2(i–k).

The 2D EWLPS method is applied across the axial slices to obtain the bone enhancement of the given US volume, therefore, a better bone enhancement is expected across the axial slices than across the other directions. Figure 2(i) demonstrates a better registration accuracy in axial direction compared to the sagittal one (solid vs dash arrow) for the EWLPS method. The 3DLPS method mainly fails to enhance the curvy surfaces (an example in Fig. 2(c)), as a result, it leads to less accuracy in registration to the curvy surfaces (Fig. 2(j)).

4   Discussion and Conclusion

We have presented a bone enhancement method for 3D US volumes based on the utilization of local 3D spectrum variation. The introduction of the spectrum variation in the filter design allows us to estimate the 3D local phase symmetry more accurately, subsequently better enhancing the expected bone locations. The improved bone enhancement in turn allows a better statistical model registration to the US volume. We have applied our technique to 13 cadaver wrists, and obtained an average mSDE of 0.7 mm and an average mxSDE of 1.8 mm between the registered and reference scaphoid bone surfaces. Though our mxSDE

improvement of 0.5 mm is small in absolute magnitude, the achieved improvement is significant at about 25 % of the clinical surgical accuracy (2 mm).

The appearance of neighboring bones in the US volume has a significant impact on the registration accuracy. We have observed better registration accuracies where the scaphoid and all of its four neighboring bones (lunate, trapezium, capitate, part of radius) are included in the field of view of the US scans.

The tuning parameter (T_{bone}) acts as a trade-off between the appearance of the bony anatomy and the outlier in the extracted surface. We have selected T_{bone} in such a way that more outliers are allowed with the purpose of increased bone visibility. The effect of the outlier has been compensated by using a probabilistic registration approach that was robust to noise and outliers.

One of the limitations of the proposed approach is enhancement of the symmetrical noise. This type of noise mainly appears as scattered objects (marked by circles in Figs. 2(d), (h)) in the bone enhanced volumes. Another limitation is ineffective shadow information utilization. The shadow map used in this work was not able to reduce the non-bony responses substantially.

Future work includes the development of a post-filtering approach on the bone enhanced volume to remove the scattered outliers. We also aim to integrate the proposed technology in a clinical workflow and compare it with a fluoroscopic guidance-based technique. Further improvement of the run-time is also needed for the clinical implementation.

References

1. Anas, E.M.A., et al.: A statistical shape+pose model for segmentation of wrist CT images. In: SPIE Medical Imaging, vol. 9034, pp. T1–8. International Society for Optics and Photonics (2014)
2. Anas, E.M.A., et al.: Bone enhancement in ultrasound using local spectrum variations for guiding percutaneous scaphoid fracture fixation procedures. IJCARS **10**(6), 959–969 (2015)
3. Beek, M., et al.: Validation of a new surgical procedure for percutaneous scaphoid fixation using intra-operative ultrasound. Med. Image Anal. **12**(2), 152–162 (2008)
4. Foroughi, P., Boctor, E., Swartz, M.: 2-D ultrasound bone segmentation using dynamic programming. In: IEEE Ultrasonics Symposium, pp. 2523–2526 (2007)
5. Hacihaliloglu, I., et al.: Automatic bone localization and fracture detection from volumetric ultrasound images using 3-D local phase features. UMB **38**(1), 128–144 (2012)
6. Hacihaliloglu, I., et al.: Local phase tensor features for 3D ultrasound to statistical shape+pose spine model registration. IEEE TMI **33**(11), 2167–2179 (2014)
7. Menapace, K.A., et al.: Anatomic placement of the herbert-whipple screw in scaphoid fractures: a cadaver study. J. Hand Surg. **26**(5), 883–892 (2001)
8. van der Molen, M.A.: Time off work due to scaphoid fractures and other carpal injuries in the Netherlands in the period 1990 to 1993. J. Hand Surg.: Br. Eur. **24**(2), 193–198 (1999)

9. Moore, D.C., et al.: A digital database of wrist bone anatomy and carpal kinematics. J. Biomech. **40**(11), 2537–2542 (2007)
10. Navab, N., Heining, S.M., Traub, J.: Camera augmented mobile C-arm (CAMC): calibration, accuracy study, and clinical applications. IEEE TMI **29**(7), 1412–1423 (2010)
11. Rasoulian, A., Rohling, R., Abolmaesumi, P.: Lumbar spine segmentation using a statistical multi-vertebrae anatomical shape+pose model. IEEE TMI **32**(10), 1890–1900 (2013)